Multiferroic perovskites under epitaxial strain

Daumont, Cristophe

Chapter 1

General introduction

1.1 Multiferroic materials

Multiferroic materials form a special class of materials exhibiting coexistence of two or more ferroic orders (ferromagnetism, ferroelectricity and ferroelasticity) [1–8]. This coexistence is difficult to achieve for various reasons. On the one hand, in most conventional ferroelectrics, the chemical bonding, which results in an off-centre position of the transition metal ions creating electric polarization, requires a formally empty d-electron configuration. On the other hand, ferromagnetism requires unpaired d-electrons. Then, the coexistence of the two properties seems incompatible with the local chemistry [2]. Therefore, non-conventional mechanisms are required to explain the occurrence of multiferroicity in materials and to create new multiferroics.

Initially, partial substitution of ferroelectrics with paramagnetic cations was proposed [9]. In this case, the requirements for the d-shell are met, and one crystallographic site may contain both an empty d-shell cation and a partially filled d-shell cation [9]. Examples of this mechanism are compounds such as $PbFe_{1/2}Nb_{1/2}O_3$ [10] and $PbFe_{1/2}Ti_{1/2}O_3$ [11]. Another mechanism leading to multiferroic behaviour is using the stereochemical activity of Bi^{3+} and/or Pb^{2+} "lone pairs", as in the case of $PbVO_3$, $BiFeO_3$ or $BiMnO_3$, although the multiferroic nature of $BiMnO_3$ is still disputed [12–23]. In these compounds, the ferroelectric distortion is caused by the 6s lone pair, while Fe/Mn/V are responsible for the magnetism [2, 13, 24]. However, due to the different origin of ferroelectricity and magnetism in these materials, the coupling be-

tween these two properties is generally weak [2,3].

Other mechanisms, by which the polar state is induced by an unconventional type of ordering, can also be found. Examples are the geometric ferroelectrics, in which the structure is distorted in a complex way. Hexagonal $YMnO_3$ is an example of such a multiferroic, in which ferroelectricity is induced by a tilting of the MnO_5 bipyramids and buckling of the Y-O planes [2,25–28]. Another mechanism relates to charge ordering. In some materials, charge ordering can give rise to polarization. This was theoretically predicted for systems with intermediate site-centred and bond-centred charge ordering [29], and observed for $LuFe_2O_4$ [3, 4]. Finally, important cases, in terms of the magnitude of the coupling, are those in which the polar state is directly induced by the magnetic ordering. Examples of such systems are the spiral magnets. In these materials, the polar state arises from the breaking of inversion symmetry by a spin cycloidal structure [30]. $TbMnO_3$, the subject of this thesis, belongs to this class of spiral magnets.

A related class of materials are magnetoelectric (ME) materials. Here, a polarization (magnetization) is linearly induced by an applied magnetic (electric) field [31]. The search for materials showing the ME effect started with the prediction of a possible ME coupling [32]. This was soon afterwards observed in Cr_2O_3 [33, 34]. The ME effect is currently having a revival due to its potential for data storage and other applications [7]. Figure 1.1 shows the relationship between multiferroic and magnetoelectric materials, within the broader class of materials that are susceptible to polarize or magnetize under electrical or magnetic fields. This figure shows that not all multiferroics display ME coupling and that not all materials exhibiting ME coupling are multiferroics. However, it is believed that the largest ME couplings are to be found among the multiferroic materials. The nature of the coupling in multiferroic and magnetoelectric materials is still not fully understood and has attracted much interest in the past years, also from a fundamental perspective.

There has been renewed interest in studying the perovskite-based multiferroic materials, such as rare earth manganites $TbMn_2O_5$, $YMnO_3$, $BiMnO_3$, $HoMnO_3$ etc., which

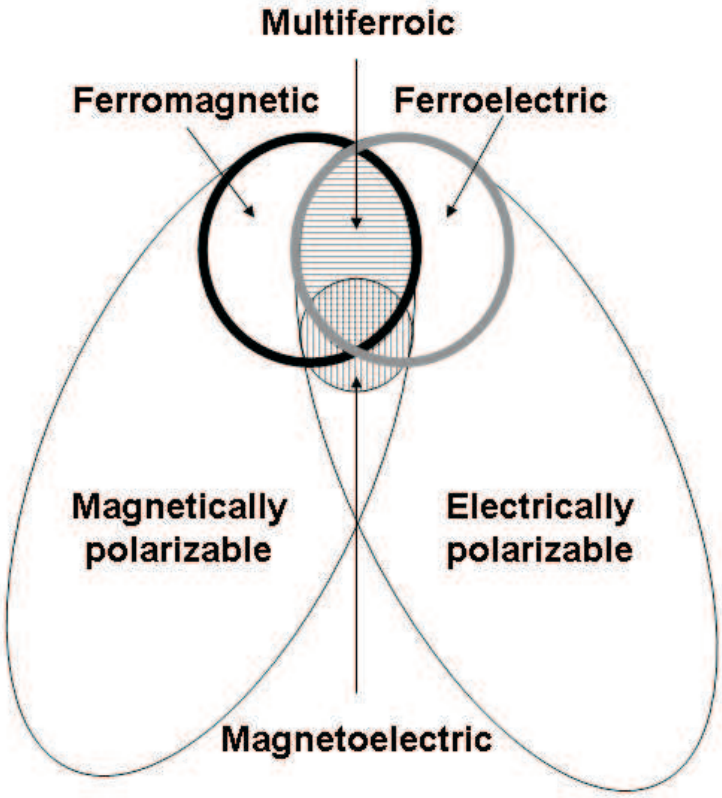

Figure 1.1: *Ferromagnetic (ferroelectric) materials have spontaneous magnetization (polarization), as shown by the black (grey) circle. The horizontally hatched region represents the multiferroics, a class of materials in which both a spontaneous polarization and magnetization are present within the same phase. The vertical hatched region shows the class of magnetoelectric materials, in which both the electrical and magnetic properties are coupled linearly to both applied electrical and magnetic fields. This figure is adapted from [7].*

have been shown to display large magnetoelectric effects. Although ferromagnetic multiferroics are preferred for applications, most of the multiferroics under investigation are antiferromagnets. This is because very few ferromagnets are good insulators, an important requirement for ferroelectricity. Moreover, recent efforts have been made to synthesize new multiferroics in the form of thin films, desirable for applications [35–37]. Interesting substrate effects, due to the epitaxial strain, can be obtained, such as stabilization of new phases that do not exist in bulk, modifications of the ferroelectric and magnetic exchange interactions or changes in electronic properties. Strain effects can be difficult to assess due to extrinsic effects, such as secondary

phases, difficulties in the synthesis of good quality materials and issues related to the characterization of very small volumes of material present in thin films. Therefore, a general explanation of the role of strain in multiferroic materials has still not been formulated. Since the main exchange interactions are sensitive to changes in the metal-oxygen bond angle and bond distances, not only the investigation of the physical response, but also an exhaustive study of the structure is essential for understanding the physics behind epitaxial strain effects.

1.2 Perovskite-based compounds

When attempting epitaxy, the relatively simple chemistry and structure of perovskites is very helpful. Moreover, several ferromagnets, various ferroelectrics and some of the most popular multiferroic materials are perovskites.

The general formula for perovskite-based materials is ABO_3, where A and B are cations with different sizes and/or valences. The B cation is located at the centre of 6 oxygen atoms with a octahedral coordination. The ideal perovskite structure is cubic, as shown in figure 1.2 (a). The distortion of the perovskites from the cubic symmetry is measured by the so-called tolerance factor, defined by Goldschmidt in the early 1920's [38], and expressed as:

$$t = \frac{r_A + r_O}{\sqrt{2}(r_B + r_O)} \tag{1.1}$$

where r_A, r_B and r_O are the ionic radii of A cation, B cation and oxygen O, respectively. Almost all perovskites have a tolerance factor between 0.75 and 1. Moreover, the distortion of the unit cell increases as the tolerance factor decreases from 1 (the tolerance factor for an ideal cubic perovskite).

1.3 Structure of bulk $TbMnO_3$

The perovskite terbium manganite has an orthorhombic unit cell (space group: Pbnm), as shown in figure 1.2 (b), a tolerance factor of 0.89, and lattice parameters of a_o = 5.2931 Å, b_o = 5.8384 Å, and c_o = 7.4025 Å [39]. The lattice parameters reported for bulk/single crystal samples, in particular the c-lattice parameter, vary significantly. This variation has been attributed to different growth conditions and it is most likely due to different oxygen contents [40–42]. The unit cell is rotated by 45^o around the c-axis, with respect to the primitive cubic cell, it is doubled along the c axis and multiplied by $\sqrt{2}$ along the a and b-axis. The unit cell thus contains 4 formula units (see figure 1.2 (b)).

This is due to the distortion and tilt of the oxygen octahedra (antiphase rotation of the oxygen octahedra along the a and b axes of the pseudo cubic unit cell and the in-phase rotation along the c axis of the pseudocubic unit cell), which is known as $GdFeO_3$ distortions [43, 44]. The in-phase and antiphase rotations of the oxygen octahedra, in the space group Pbnm, can be described as $a^-a^-b^+$, using the Glazer notation [45]. This type of distortion is associated with orthorhombic lattice parameters that follow the relationship $c_o/\sqrt{2} > a_o$ and $a_o < b_o$. The lattice parameters, in the case of $TbMnO_3$, have a different relationship ($c_o/\sqrt{2} < a_o$), indicating that the Pbnm structure of $TbMnO_3$ presents another distortion superimposed on the $GdFeO_3$-like rotations.

Indeed, the manganese ions in the structure are in an octahedral coordination and possess a valence of 3+. In the high spin state (S=2), three electrons occupy the t_{2g} orbitals and one electron occupies the doubly degenerate e_g orbitals. This implies that the high spin state of manganese in $TbMnO_3$ is Jahn-Teller active (see table 1.1) [46]. Moreover, the manganese ions can also exist in a low spin state (S=1) with 4 electrons occupying the t_{2g} orbitals, leading to a weak Jahn-Teller effect in this spin state (as shown in table 1.1).

The Jahn-Teller effect is most pronounced when an odd number of electrons oc-

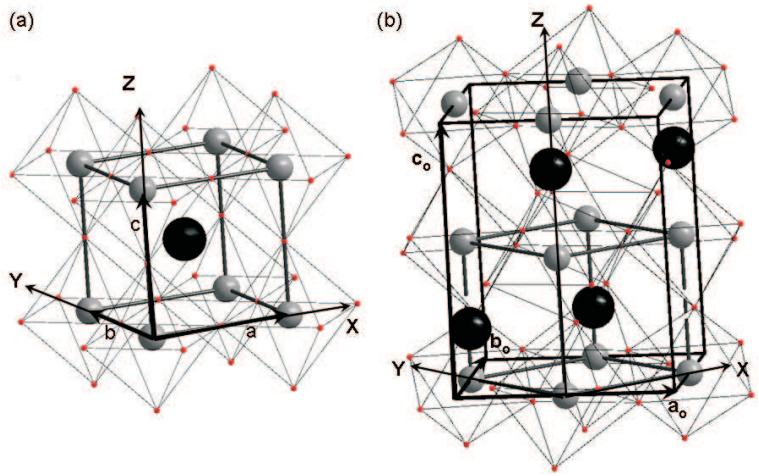

Figure 1.2: *(a) Crystal structure of ABO_3 in its cubic form. (b) Crystal structure of $TbMnO_3$ in its room temperature orthorhombic symmetry, as indicated by black contour. The pseudo cubic unit cell is drawn inside the orthorhombic unit cell as grey contour.*

Table 1.1: *Strength of the Jahn Teller effect in an octahedral TM-O_6 complex considering the number of electrons in the d orbitals of the transition metal TM. s=strong effect; w=weak effect.*

number of electrons	1	2	3	4	5	6	7	8	9	10
High spin	w	w	-	s	-	w	w	-	s	w
Low spin	w	w	-	w	w	-	s	-	s	-

cupy the e_g orbitals. This is because the e_g orbitals point directly at the coordinating oxygen atoms. The effect also occurs for a strong degeneracy of electrons in the t_{2g} orbitals. However, the effect is much less noticeable than when e_g orbitals are involved, because the t_{2g} orbitals do not point directly in direction of the coordinating oxygens. The expected effects for an octahedrally coordinated system are given in table 1.1.

The Jahn-Teller effect leads to distortions of the oxygen octahedron as shown in figure 1.3.

Another effect of the Jahn Teller distortion is the lifting of degeneracy of the e_g orbitals, stabilizing the d_{z^2} or $d_{x^2-y^2}$ orbitals depending on if the Jahn-Teller distortion compresses or expands one of the directions of the oxygen octahedra (Q3 mode).

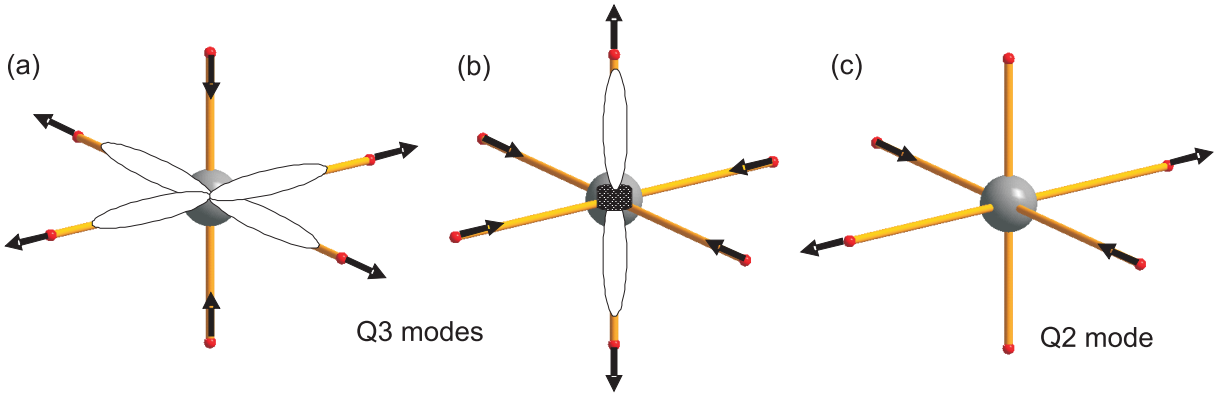

Figure 1.3: *(a), (b) Two different types of Q3 mode of Jahn-Teller distortion stabilizing the $d_{x^2-y^2}$ and d_{z^2}, respectively. (c) Q2 mode of the Jahn-Teller distortion favouring a superposition of $d_{x^2-y^2}$ and d_{z^2}.*

Compression in the (ab)-plane stabilizes the d_{z^2} orbital whereas expansion stabilizes the $d_{x^2-y^2}$ orbital, as shown in figure 1.3 (a) and (b). The Jahn-Teller distortion can also produce an effect of orthorhombic distortion of the oxygen octahedra (Q2 mode), stabilizing a superposition of the d_{z^2} and $d_{x^2-y^2}$ orbitals (as shown in figure 1.3 (c)). In the case of $TbMnO_3$, the longest Mn-O bond is on the (ab) plane, whereas the shortest Mn-O bond is along the out-of-plane direction. This means that the $d_{3x^2-r^2}$ and $d_{3y^2-r^2}$ orbitals are stabilized in $TbMnO_3$ as shown in figure 1.4 (a). Finally, a cooperative Jahn-Teller distortion in a thin film under epitaxial strain might influence the cation-ligand-cation superexchange interactions; this is further described in the next section.

1.4 Superexchange and double-exchange interactions.

The magnetic interactions in $TbMnO_3$ are dominated by the so-called 'superexchange'. Superexchange is the magnetic coupling between two ions (Mn^{3+}) through a nonmagnetic intermediate anion (O^{2-}) and was originally proposed by Kramers in 1934. He noticed that in crystals like MnO, the Mn atoms interact magnetically despite having a nonmagnetic oxygen ion between them [47]. Anderson later refined Kramers' model [48]. The main features of the superexchange interactions are usually summa-

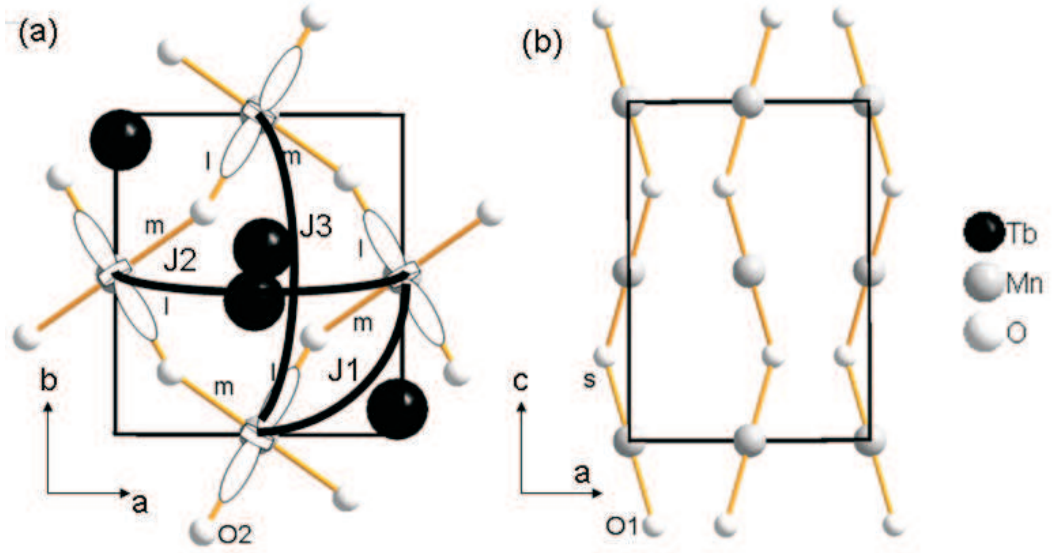

Figure 1.4: *(a) Representation of the structure of $TbMnO_3$ in the (ab) plane. The alternating medium and long bond length are indicated as 'm' and 'l', respectively. The stabilized $d_{3x^2-r^2}$ and $d_{3y^2-r^2}$ are represented by their classical shape. The NN and NNN superexchange interactions are shown in the picture, denoted by J1 (nearest neighbour superexchange), J2 (next nearest neighbour along a) and J3 (next nearest neighbour along b). (b) Representation of the structure of $TbMnO_3$ in the (ac) plane. The short bond length is indicated a 's' in the picture. This representation emphasizes the tilting of the oxygen octahedra along the c axis of the structure.*

rized by the so-called 'Goodenough-Kanamori-Anderson (GKA)' rules. According to these rules, the 180^o superexchange between two magnetic ions, in which the magnetic ion-ligand-magnetic ion angle is closest to 180^o, is strongly antiferromagnetic. The 90^o superexchange (magnetic ion-ligand-magnetic ion angle close to 90^o) interaction is weakly ferromagnetic. Moreover, the 180^o superexchange is maximum for an angle of 180^o, allowing maximum overlap of the relevant orbitals. The 180^o superexchange becomes weaker as the angle decreases [49].

The GKA rules are valid for transition metals that are not Jahn-Teller active. For Jahn-Teller distorted systems, the 180^o superexchange rules are different. Superexchange adheres to the quantum mechanic requirement of an antisymmetric total wave function. For cooperatively Jahn-Teller distorted perovskites, the antisymmetric wave function is imposed by the antiferrodistorted structure. The latter is the result of the corner-sharing octahedra of the perovskite structure, as described in the previous sec-

tion. Thus, the orbital part of the wave function imposes the antisymmetric symmetry and thus the magnetic interaction is ferromagnetic in the a-b basal plane. For Pbnm-symmetry perovskites, the mirror symmetry perpendicular to the c-axis results in the same orbital occupation along the c-axis. This imposes antiferromagnetic interactions along the c-axis.

Besides superexchange, there is another interaction for mixed valence compounds. E.g. for Mn^{3+}-O-Mn^{4+} fragments, charge transport results in a stabilization of the ferromagnetic interactions. This mechanisms operates for doped compounds and is known as double-exchange. Here, it involves the simultaneous charge transfer of an electron from Mn^{3+} to O^{2-} and another from O^{2-} to Mn^{4+}. For high enough doping, it can lead to a metallic ferromagnetic state as e.g. in $La_{1-x}Ca_xMnO_3$ for $0.2 < x < 0.5$.

1.5 $TbMnO_3$ and its complexity.

In bulk form, $TbMnO_3$ is one of the most popular multiferroics. In manganites, the magnetic ground state as a function of the size of the A-site cation shows a rich behaviour that gives rise to different magnetic structures. Changing the size of the A-site cation by choosing different rare earth ions is known as applying 'chemical pressure'.

The magnetic structure of bulk $TbMnO_3$ is complicated and is the result of the competition between ferromagnetic (FM) and antiferromagnetic (AFM) interactions, leading to frustration and incommensurability of the spin structure. This competition arises as the Mn-O-Mn bond angle gives rise to intermediate interactions between antiferromagnetic 180^o superexchange and ferromagnetic 90^o superexchange [49]. This material is then an interesting candidate for studying the effect of epitaxial strain. Indeed, as shown in figure 1.5, $TbMnO_3$ lies in between two different magnetic structures. For Mn-O-Mn bond angles higher than 146^o, an A-type antiferromagnetic structure is found, as in the case of $LaMnO_3$ [51]. For bond angles lower than 144^o, an E-type antiferromagnetic structure is found, as in the case of $HoMnO_3$ [52]. Both A-type

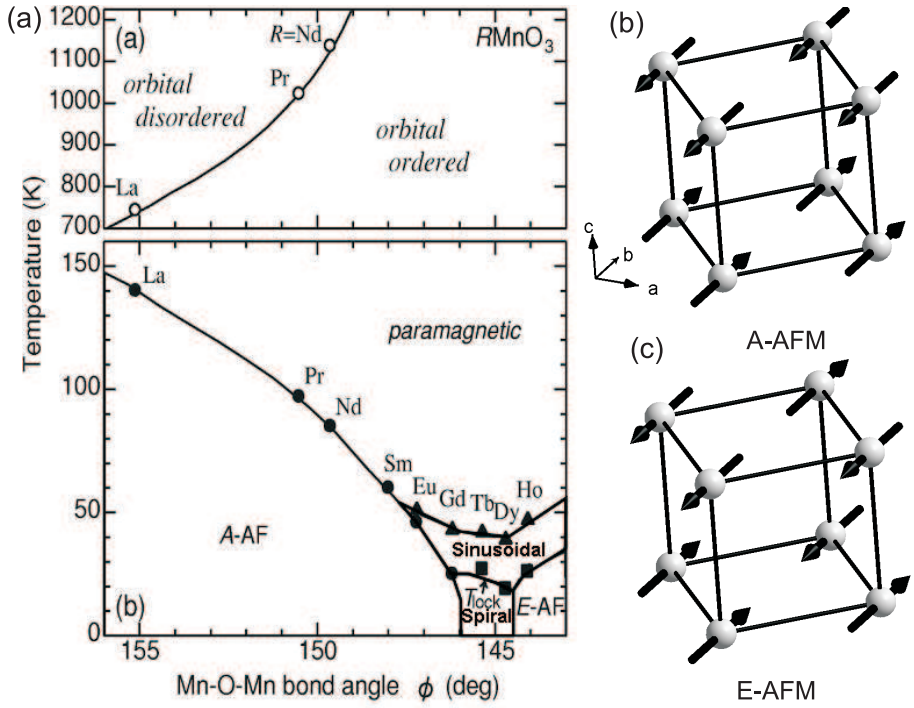

Figure 1.5: *(a) Magnetic phase diagram for orthorhombic rare earth manganites showing temperature as a function of the Mn-O-Mn bond angle. The figure is taken from [50]. $TbMnO_3$ lies in an intermediate region between the A-type (b) and E-type (c) antiferromagnetic magnetic structures. Moreover, the upper plot shows that all the rare earth manganites are orbitally ordered at room temperature.*

and E-type are schematically shown in figure 1.5 (b) and (c), respectively. At smaller ionic radii (not shown in the figure), the hexagonal crystallographic structure is more stable but it is outside the scope of this thesis. Moreover, the rare earth manganites $RMnO_3$ (from La to Ho) are all orbitally ordered at room temperature, because of the Jahn-Teller active Mn^{3+} ion with an increasing ordering temperature as the ionic radius is decreased [53]. The orbital ordering temperature for $TbMnO_3$ is of the order of 1500K [53].

The magnetic structure of $TbMnO_3$ has been exhaustively studied [40, 50, 54] and it is shown to display an incommensurate antiferromagnetic sinusoidal spin ordering below 40K. A transition to a non-collinear antiferromagnetic cycloid spin ordering along the b-direction follows below 27K (see figure 1.6). Phenomenologically, a way to generate the cycloidal phase is to consider that the ferromagnetic nearest-

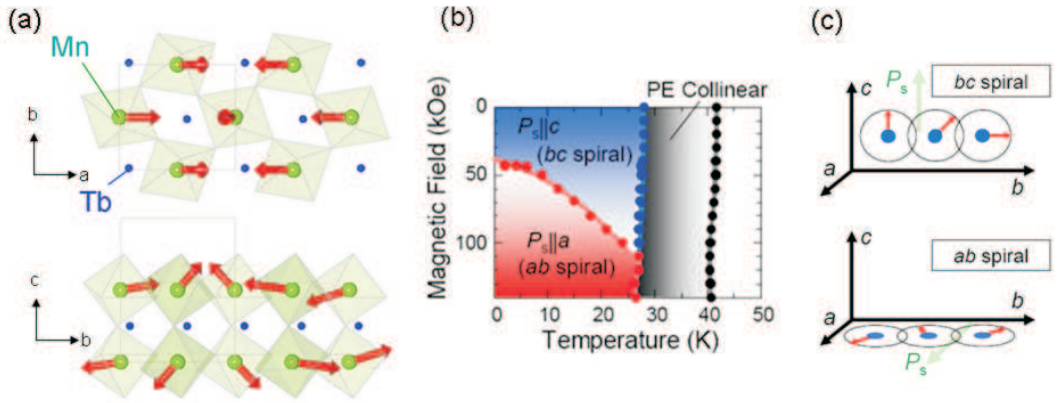

Figure 1.6: *(a) Magnetic structure of $TbMnO_3$ in the spin cycloid state. The spin cycloid is indicated by arrows and projected in the (a,b) plane (top panel) and (b,c) plane (bottom panel). (b) Applied magnetic field versus temperature phase diagram for $TbMnO_3$. (c) Schematic representation of the polarization flip transition under field. The figure is adapted from references [58, 59]*

neighbour (NN) superexchange is frustrated by a sufficiently strong antiferromagnetic next-nearest-neighbour (NNN) superexchange, allowing for the observed incommensurability of the magnetic structure with respect to the lattice periodicity [3]. This is the so-called J1-J2-J3 model, using classical spins, where J1 is the NN superexchange, J2 and J3 are the NNN superexchange along the a and b directions, respectively, as shown in figure 1.4 [55].

The cycloid phase requires the Lifshitz invariants in the Landau free energy [56]. Using Landau free energy, it has be shown that the cycloidal ordering breaks the inversion symmetry and allows for a polarization, perpendicular to both the wave vector ($\vec{q}$) and the spin rotation axis ($\vec{e_3}$) of the cycloid (P $\propto \vec{e_3}$x$\vec{q}$) [30, 40, 57]. In the case of $TbMnO_3$, the wave vector is along the b-axis and the spin rotation is around the a-axis, as shown in figure 1.6. Therefore, the experimentally observed polarization along the c-direction confirms the theory.

Microscopically, two possible mechanisms have been used to explain the appearance of the ferroelectric polarization at the cycloidal ordering: (a) An electronic contribution due to spin-orbit coupling [60, 61] and (b) a cation displacement due to the inverse Dzyaloshinskii-Moriya (DM) interaction (P $\propto \vec{D}.(\vec{S_i}x\vec{S_j})$) [62, 63]. Recently,

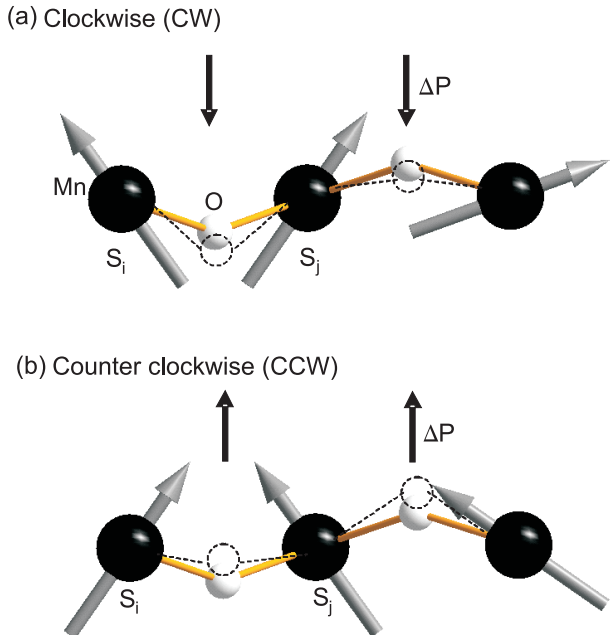

Figure 1.7: *(a) Schematic drawing of the local polarization in a clockwise cycloid (a) and in a counter-clockwise cycloid (b). The related local electric polarizations are shown as black arrows. The spins are indicated as grey arrows, whereas the manganese and oxygens atoms are represented by black and white spheres, respectively. The shifts of oxygen atoms, due to the spin canting of neighbouring atoms, are indicated as dashed lines. Figure adapted [69]*

however, it has been theoretically shown that the inverse effect of the Dzyaloshinskii-Moriya interaction [64,65], and its related atomic displacement, is the mechanism that explains the emergence of a net ferroelectric polarization in $TbMnO_3$ [66–68].

Indeed, the cycloidal arrangement of the spins induces an orientation of the local electric polarizations along the same direction, due to the inverse DM interaction, and allows for a net macroscopic polarization, as shown in figure 1.7 (a), for the case of a clockwise cycloidal. Moreover, it is also expected, that due to the asymmetric DM interaction $[(\vec{S_i}\mathrm{x}\vec{S_j})\text{=-}(\vec{S_j}\mathrm{x}\vec{S_i})]$, the polarization can be switched by time reversal of the cycloid, as shown in figure 1.7 (b) for a counter-clockwise cycloid. In the case of a cycloidal ordering, a strong coupling can be expected between the electric and magnetic orders, as they are associated with a single mechanism. Even though cycloidal spin structures and related polarizations usually appear at low temperatures, such systems are of special fundamental interest because of this large coupling be-

tween the magnetic and electric orders, and the fundamental challenges they pose. Indeed, it has been shown for $TbMnO_3$ that a field of around 5T along the a-direction flips the spin rotation axis and simultaneously the polarization, from the c-axis to the a-axis [54, 70](as shown in the phase diagram in figure 1.6(b) and sketched in figure 1.6(c)).

1.6 Manganites thin films

Studies of rare earth manganites ($RMnO_3$, R=rare earth ion) in thin film form started to be available only since 2006 and have been performed in various compositions for R changing from La to Ho. The most studied being $LaMnO_3$, due to its colossal magnetoresistance observed in bulk, upon doping by Sr or Ca. Only the multiferroic rare earth manganites close to $TbMnO_3$ (i.e. R = Gd, Ho, Y, Yb, Tb) will be discussed here. In particular, we focus on several reports that reveal induced or enhanced ferromagnetic interactions, which are absent in the bulk [71–80].

Among them, orthorhombic $HoMnO_3$ films of about 150nm [71] and 200nm [72] have been deposited on (001)-$SrTiO_3$ by pulsed laser deposition. In both cases, a split between the zero-field-cooled (ZFC) and the field-cooled (FC) of the magnetization-temperature curves is observed below the antiferromagnetic transition (occurring at the same temperature as the bulk) [71, 72]. In the work of J.G. Lin *et al.*, the ZFC-FC splitting was attributed to a field induced magnetization in the region of incommensurate to commensurate spin structure [72]. It is worth to note that two types of crystallographic domains were present in the films. T.H. Lin *et al.* suggested that the ZFC-FC splitting was due to weak ferromagnetism [71]. Although no clear statement is offered about its nature, two possible origins were discussed: One relates the weak ferromagnetism to spin canting and the other one to uncompensated spins at the boundaries of AFM domain walls [71], giving as example the weak ferromagnetism observed in AFM nanoparticles [71, 81]. These reports are very recent and the origin of the weak

ferromagnetism has yet to be confirmed.

Epitaxial stabilization of metastable structures is also possible. $YMnO_3$ was grown on $SrTiO_3$ with an orthorhombic (o-)structure by *X. Marti et al.* [73] by using pulsed laser deposition. A ZFC-FC hysteresis was also found below the antiferromagnetic ordering temperature, associated with a ferromagnetic response [73]. Roughness effects were suggested but experimentally discarded whereas the strain state (and specially the contraction of the b-axis) of the films was suggested as the likely origin [73]. Another report on o-$YMnO_3$ thin films grown on $SrTiO_3$ also showed a splitting between zero field cooled (ZFC) and field cooled (FC) curves below the antiferromagnetic transition [74]. The authors tentatively suggest that a strain-induced canted AFM state, for thin films, instead of the incommensurate to lock-in transition reported for bulk samples, is occurring [74]. Roughness effects were also suggested to account for the ferromagnetic interactions observed in the epitaxially grown thin films of o-$YbMnO_3$ [75].

When decreasing the ionic radius of the rare earth in bulk $RMnO_3$ compounds beyond R=Dy, the stable crystalline phase changes from orthorhombic to hexagonal [50]. Contrary to the orthorhombic phase, in which the ferroelectric ordering originates from the magnetically-induced lattice modulation, the ferroelectricty in hexagonal manganites arises from the tilting of the MnO_5 bipyramids [25]. Over the last few years, a wide variety of hexagonal/orthorhombic rare earth manganites (h-$RMnO_3$ have been grown in thin film form (including studies with R=Nd, Ho, Tm, Lu, Yb, Gd, Tb) [76–78, 80, 82]. However, hexagonal manganites under epitaxial strain are not the scope of this thesis.

The examples described above show that induced/enhanced magnetization was consistently reported for different manganite thin films in the last couple of years, a clear explanation has not been offered yet and a general origin for the induced ferromagnetism observed in epitaxially stabilized $RMnO_3$, specially those with similar ionic radii, cannot be discarded.

1.7 Outline of this thesis

This thesis addresses the role of strain on the multiferroic behaviour of orthorhombic rare earth manganites, focusing on $TbMnO_3$. As explained above, the structural distortion of the orthorhombic perovskite unit cell can lead to large modifications of the ferroelectric, magnetic and electronic properties of rare earth manganites. The advantage of the thin films is that they allow to change the crystallographic structure without modifying the cation on the rare earth site. This permits a detailed understanding of the relationships between the structure and the physical properties in thin film form. In particular, we have dedicated special effort to reveal the origin of the ZFC-FC hysteresis, observed in thin films of $TbMnO_3$ and that could be a more general effect of strain in orthorhombic manganites (see previous section). The ultimate goal is to try to tune the physical properties of the material using epitaxial strain, imposed by the substrate.

Although films of $TbMnO_3$ have been previouly grown by Cui *et. al.* [83–85], these were polycrystalline and not strained. Thin films of $TbMnO_3$ under epitaxial strain have been deposited in this thesis for the first time, using pulsed laser deposition on single crystals of (001)-oriented $SrTiO_3$ (after the publication of our results, a second, less exhaustive, report on epitaxially grown $TbMnO_3$ has been published by other authors [86]. Thin films of $TbMnO_3$ were also deposited on $SrRuO_3$ buffered (001)-oriented single crystals of $DyScO_3$ for the first time, during this thesis. Detailed structural, magnetic and dielectric characterization has been performed in order to answer the following main questions:

- What are the structural modifications by the strain induced from the substrate?
- How does strain affect the ferroic properties and the magnetoelectric coupling?
- Can the properties be systematically tuned by strain?
- What can we learn from the thin film behaviour of $TbMnO_3$ about the properties of multiferroics and manganites in general?

The thesis is organized as follows: Chapter 2 describes the experimental techniques used in this thesis. Chapter 3 presents the growth and a detailed structural characterization of $TbMnO_3$ thin films grown on $SrTiO_3$, using synchrotron and high resolution laboratory x-ray diffraction, as well as TEM. Chapter 4 describes the magnetic and electronic properties of the films, characterized using SQUID magnetometer and x-ray photoelectron spectroscopy; Chapter 5 reports the dielectric and magnetoelectric response of the $TbMnO_3$ thin films grown on $SrTiO_3$. Finally, Chapter 6 presents the growth and characterization of $TbMnO_3$ thin films on $SrRuO_3$ buffered $DyScO_3$ substrates. The chapters are designed such that they can be read independently.